sustainability

MDPI

Article

Research on a Non-Synchronous Coordinated Reduction Method for Slopes Based on the Hoek–Brown Criterion and Acoustic Testing Technology

Li He [1,2,3], Yongming Zhao [2,*], Lin Yin [2], Dongwang Zhong [2], Haitao Xiong [2], Shasha Chen [2] and Xinyue Zhang [2]

[1] Hubei Key Laboratory of Systems Science in Metallurgical Process, Wuhan University of Science and Technology, Wuhan 430065, China; heli86@wust.edu.cn
[2] College of Science, Wuhan University of Science and Technology, Wuhan 430065, China; ylyinlin@outlook.com (L.Y.); zhongdw123@263.net (D.Z.); 17772103902@163.com (H.X.); chenshashacc@icloud.com (S.C.); zxydyj133999@163.com (X.Z.)
[3] Hubei Key Laboratory of Blasting Engineering, Jiang Han University, Wuhan 430056, China
* Correspondence: zhaoym0404@163.com

Abstract: In the process of the evolution of rocky slope instability, the decay deterioration rate of cohesion c and internal friction angle φ are different, and there are also differences in the order and degree of their impact on slope stability; thus, it is of great theoretical value to propose a more practical calculation method for the reduction in slope degradation. This paper combines the Hoek–Brown criterion and an acoustic test method to estimate the mechanical parameters of slope rock mass; the correlative relationship within the double-strength parameter reduction was established by introducing advanced reduction steps (ARS), n, and correlation factor, λ, and a non-synchronous coordinated reduction (NSCR) method for the double parameters of slopes was proposed. Furthermore, methods for determining the comprehensive safety factor (CSF) of slopes during the coordinated reduction of double parameters are comparatively analyzed. The results of the application of engineering examples show that the strength of the slope rock mass is significantly reduced after several blast disturbances, and the equivalent cohesion is reduced from 1.05 MPa to 0.89 MPa, while the internal friction angle is reduced from 25.68° to 21.77°. The CSF calculated using the W. Yuan-2 method is closer to the results of the limit equilibrium method and is suitable for the calculation of the CSF of the NSCR of slopes. The slope CSFs show a trend of first increasing and then decreasing with the increase in n; F_S = 3.349 when n = 50, with a relative error of only 8.1% compared to the results calculated using the limit equilibrium method. The NSCR method remediates the blindness of the traditional strength reduction method in double-parameter reduction and ensures that the reduction range of the internal friction angle is no lower than its residual strength limit value, making it practical and feasible for slope stability analysis.

Keywords: slope stability; Hoek–Brown criterion; acoustic testing; non-synchronous coordinated reduction; limit equilibrium method

check for updates

Citation: He, L.; Zhao, Y.; Yin, L.; Zhong, D.; Xiong, H.; Chen, S.; Zhang, X. Research on a Non-Synchronous Coordinated Reduction Method for Slopes Based on the Hoek–Brown Criterion and Acoustic Testing Technology. *Sustainability* **2023**, *15*, 15516. https://doi.org/10.3390/su152115516

Academic Editor: Anjui Li

Received: 5 September 2023
Revised: 22 October 2023
Accepted: 25 October 2023
Published: 1 November 2023

Copyright: © 2023 by the authors. Licensee MDPI, Basel, Switzerland. This article is an open access article distributed under the terms and conditions of the Creative Commons Attribution (CC BY) license (https://creativecommons.org/licenses/by/4.0/).

1. Introduction

Mining, road construction, and other projects mostly need blasting technology for excavation and construction; however, meeting the needs of said projects will at the same time inevitably produce a variety of hazardous effects [1–3] such as blasting vibration, blasting fly rock, and blasting shock waves [4,5]. Blasting vibration is one of the most significant hazardous effects [6,7], affecting the stability of the surrounding slope body, even causing slope instability and collapse, which can result in safety accidents and economic losses; thus, reasonable slope stability analyses are of great significance [8,9].

The limit equilibrium method, as one of the most commonly used methods for slope stability analysis [10–12], particularly in combination with intelligent optimization algorithms (such as the limit equilibrium method, combining improved ant colony algorithms and genetic algorithms [13]; and particle swarm algorithms, incorporating immune selection and inoculation mechanisms [14]), improves the computational efficiency and accuracy of the analysis. However, due to defects in the limit equilibrium method itself, it is neither able to deal with extremely complex slopes, nor able to assume the sliding surface in advance; smeanwhile, the finite element method can offset this defect very well [15]. Shao et al. [16] combined these two methods. The finite element strength reduction method, first proposed by Zienkiewicz et al. [17] in 1975, can deal with slope profiles with complex geometries, boundaries, and loading conditions, and nonlinear stress–strain relationships [18–21]. It does not require prior assumption of sliding surfaces; in addition, it can characterize the deformation, displacement, and stress–strain of slopes. However, the traditional strength reduction method implements the strength parameters of cohesion, c, and internal friction angle, φ, in the same proportion for the calculation of the reduction. The parameters of cohesion (c) and the internal friction angle (φ) maintain consistent weakening and contribution ratios throughout the progressive degradation of the geotechnical body; in this way, the aforementioned process may appear straightforward. However, it fails to align with actual slope failure phenomena [22–26]. Practical experiments have shown that the cohesion (c) and the internal friction angle (φ) do not reach their peak strength and critical limit at the same time, and different reduction coefficients should be used for the double-parameter reduction with respect to the double-strength parameter characteristics and weakening mechanisms [27,28]. In addition, the internal friction angle (φ) cannot be reduced without any limitation, and it needs to satisfy $\sin \varphi \geq 1 - 2\mu$ [29]. Tang et al. [30] firstly proposed the concept of the double-parameter reduction of slopes. Although their approach was based on the limit equilibrium method, Jiang et al. [31] pointed out the reasonable value of the double-reduction coefficients for isotropic soil slopes. Yuan et al. [32] conducted a study using arithmetic examples to examine the relationship between double-reduction coefficients in various slope conditions. Additionally, they proposed two distinct methods for defining the integrated factor of safety. Isakov and Moryachkov [33] established an equation of the relationship between the integrated safety factor and the strength reduction path. Afterwards, Xue et al. [34] proposed a double-parameter non-proportional strength reduction method based on the finite element method. They established a non-proportional reduction relationship between double-strength parameters, assuming that the cohesion c and the internal friction angle φ decay linearly. However, they did not consider the reduction order of the double parameters. Terzaghi and Peck [35] proposed that in the process of the progressive failure of slopes, cohesive strength c and internal friction angle φ do not fail simultaneously. Chen et al. [36] proposed a local dynamic reduction method to represent this process, but they did not consider different reduction coefficients for the double-strength parameters.

The mechanical parameters of the slope rock mass need to be determined before the slope stability analysis, and the deformation parameters and mechanical behavior of the rock mass are the basis for the implementation and safety assessment of all kinds of geotechnical engineering projects, being thereby related to the construction of engineering projects, economic benefits, and safety [37,38]. A widely used empirical estimation method is the Hoek–Brown criterion, which integrates various structural features describing the deformability and strength of a rock mass [39,40], where the important parameters to be estimated are the geological strength index, GSI, and the disturbance factor, D. The estimation method was also provided by Hoek et al. [41,42], who also plotted its conditions and range of use. Due to the qualitative estimation of parameters, which lacks some rigor, it is still difficult to quickly and accurately determine the mechanical parameters of the rock mass. The method of large-scale in situ testing [43,44], as a method for determining the mechanical parameters of rock mass, calculates results with high accuracy and allows direct determination of the strength and deformation properties of the rock mass; however, the

method is quite expensive to test and is inefficient and time-consuming. The acoustic testing technique determines the nature of a rock body by monitoring the propagation acoustic wave velocity in the rock body, which has the advantages of being fast, simple, economical, and easy to use on a large scale. It can also be used as an effective indicator for judging the stability of the project [45–47]. According to studies conducted by scholars [48–50], the acoustic wave velocity within the rock mass is closely related to the deformation and strength parameters of the rock. Therefore, utilizing acoustic testing techniques based on the Hoek–Brown criterion has proved to be a rigorous and efficient method [51].

For this paper, we selected an acoustic testing technique based on the Hoek–Brown criterion to estimate the rock mass parameters of the slope. This methodology was chosen due to its high efficiency and economy in on-site rock mass parameter testing. Additionally, we propose an NSCR method for the slope, which is more aligned with the failure mechanism of the rock mass. This is achieved by introducing ARS n and correlation factor λ, based on the principles of the finite element strength reduction method. Finally, we verify the feasibility of the proposed method for slope stability analysis by comparing the results with those obtained using the limit equilibrium method and the strength reduction method in various examples of slope stability analysis projects.

2. Generalized Hoek–Brown Criterion

The Hoek–Brown criterion is a semi-empirical formula for rock failure mechanisms proposed by Hoek et al. [41,42], which can be used to estimate the strength and deformation trends of rock mass and has been improved and modified several times in recent decades. Furthermore, the Hoek–Brown criterion is one of the most commonly used criteria in the stability analysis of slopes. The generalized Hoek–Brown criterion for estimating rock deformation and strength can be expressed as

$$\sigma_1 = \sigma_3 + \sigma_c \left(m_b \frac{\sigma_3}{\sigma_c} + s \right)^a \tag{1}$$

where σ_1 and σ_3 represent the first principal stress and the third stress at the time of rock failure, respectively. σ_c refers to the uniaxial compressive strength of the intact rock. The other factors m_b, s, and a are material parameters related to the rock mass in the Hoek–Brown criterion, and they can be expressed as

$$m_b = m_i \exp\left(\frac{GSI - 100}{28 - 14D} \right) \tag{2}$$

$$s = \exp\left(\frac{GSI - 100}{9 - 3D} \right) \tag{3}$$

$$a = \frac{1}{2} + \frac{1}{6}\left(e^{-GSI/15} - e^{-20/3} \right) \tag{4}$$

where *GSI* is the geological strength index; the value depends on the development of joints in the rock body and the structure of the rock body, and generally, *GSI* takes a value in the range of 10–100, where 10 indicates the worst quality of the rock body and 100 indicates the best quality of the rock body. D is the disturbance factor, which indicates the degree of influence of blasting or other vibrations on the rock mass, ranging from 0 to 1. A value of 1 indicates maximum influence of the disturbance, and a value of 0 indicates that there is no disturbance effect; The value of mi depends on the type of rock involved, and for rocks with $\sigma_c/\sigma_t \geq 8$, a value of $m_i = \sigma_c/\sigma_t$ can be taken.

Hoek et al. [41,42,52] have proposed qualitative estimation methods for determining *GSI* and D. However, these methods, although fast and convenient, lack the required rigor, particularly for precise slope stability analysis. Hence, it is imperative to find a method that can provide quantitative estimations for *GSI* and D values.

3. Estimation of *GSI* and *D* Using Acoustic Testing Methods

3.1. Estimation of GSI Using Acoustic Testing Methods

There are many and quite mature studies on the seismic velocity V_p in rock bodies [53–55], and the following empirical relationships can be established through relevant statistical summaries and analyses:

$$Q = 10^{V_p - 3.5} \tag{5}$$

where Q denotes the mass index of the rock mass, and V_p denotes the seismic velocity in the rock mass.

The relationship between the RMR_{76} indicators and Q can be derived from field data and statistical analysis [56–58], and can be expressed as

$$RMR_{76} = 15\lg Q + 50 \tag{6}$$

By combining Equations (5) and (6), the relationship between the RMR_{76} index and the seismic velocity V_p can be expressed as

$$RMR_{76} = 15V_p - 2.5 \tag{7}$$

According to the linear relationship between *GSI* and RMR_{76} with $GSI = RMR_{76}$ ($RMR_{76} > 18$), the relationship between *GSI* and V_p can be expressed as

$$GSI = 15V_p - 2.5 \tag{8}$$

Wang et al. [59] found that there is a correlation between seismic velocity V_p and acoustic wave velocity C_p, which is slightly larger than the seismic velocity V_p; this relationship can be expressed as

$$C_p = 1.1V_p - 0.081 \tag{9}$$

Therefore, the relationship between the acoustic wave velocity C_p and *GSI* can be expressed simultaneously using Equations (8) and (9).

$$GSI = 13.64C_p - 1.40 \tag{10}$$

In accordance with Hoek et al. [41,42], who provided a *GSI* range of 10–90, Equation (10) may be given. When $RMR_{76} > 18$ and the acoustic wave velocity C_p is in the range of 1.4–6.7 km/s, the two satisfy the curve, as shown in Figure 1.

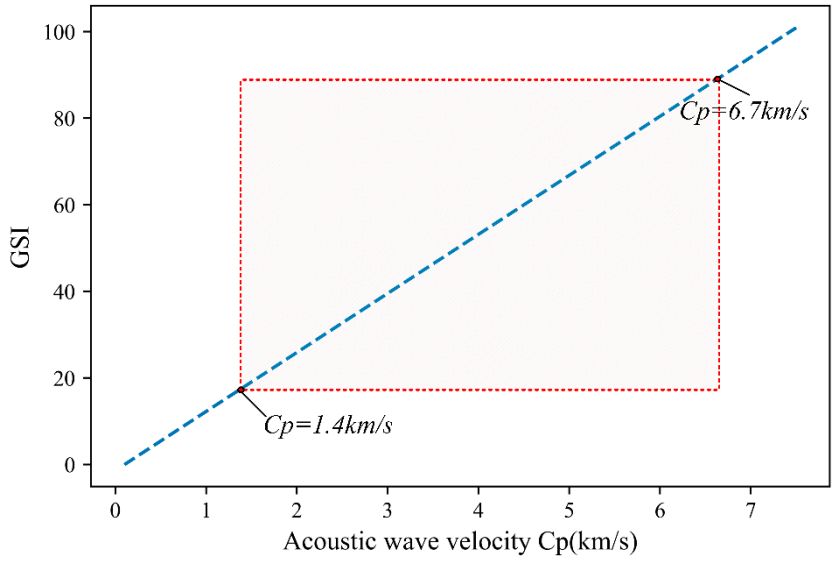


Figure 1. Curve of the relationship between *GSI* and acoustic wave velocity C_p.

3.2. Estimation of D Using Acoustic Testing Methods

The disturbance factor D, as a key parameter in response to the stress relaxation effect of the rock mass both before and after blasting disturbance, was originally used for qualitative estimation of the classical Hoek–Brown criterion [41,42]; subsequently, many scholars have attempted to find a reasonable expression for the disturbance factor D in a large number of research studies [60,61]. These scholars, including Hoek et al. [52], also presented a quantitative method of determining the value of the factor; some researchers believe that the damage factor can be directly used as the disturbance factor [62]. It has been shown [63] that the disturbance factor decreases with depth; thus, the acoustic wave velocity increases accordingly with depth, and the disturbance factor D can be determined from the change in acoustic wave velocity.

Firstly, according to the Hoek–Brown criterion, the relationship between the modulus of elasticity E_m and the disturbance factor D can be expressed as

$$E_{m.d}(GPa) = \begin{Bmatrix} \left(1 - \frac{D}{2}\right)\sqrt{\frac{\sigma_c}{100}}10^{(GSI-10)/40}(\sigma_c \le 100\text{MPa}) \\ \left(1 - \frac{D}{2}\right)10^{(GSI-10)/40}(\sigma_c > 100\text{MPa}) \end{Bmatrix} \tag{11}$$

When the rock mass is not disturbed in any way, D = 0, which can be expressed as

$$E_{m.ud}(GPa) = \begin{Bmatrix} \sqrt{\frac{\sigma_c}{100}}10^{(GSI-10)/40}(\sigma_c \le 100\text{MPa}) \\ 10^{(GSI-10)/40}(\sigma_c > 100\text{MPa}) \end{Bmatrix} \tag{12}$$

Thus, the relationship between the perturbed and unperturbed modulus of elasticity can be expressed as

$$\frac{E_{m.ud}}{E_{m.d}} = \frac{1}{1 - D/2} \tag{13}$$

According to the study conducted by Ajalleian and Mohammadi [64], the relationship between the elastic modulus (E_m) and the rock mass rating (RMR_{89}s) can be expressed as

$$E_m = E_i \exp\left(\frac{RMR_{89} - 100}{36}\right) \tag{14}$$

where the parameter E_i represents the modulus of elasticity of intact rock, unit = GPa.

The relationship between GSI and the rock mass rating RMR_{89} [65,66] can be expressed as

$$GSI = RMR_{89} - 5 \tag{15}$$

Hence, the relationship between the acoustic wave velocities C_p and the elastic modulus E_m can be expressed by simultaneously solving Equations (10), (14), and (15).

$$E_m = E_i \exp\left(\frac{13.64C_p - 96.4}{36}\right) \tag{16}$$

By combining Equations (13) and (16), the relationship between the acoustic wave velocities C_p and the disturbance factor D can be expressed as

$$D = 2\left[1 - \exp\left(-\frac{13.64(C_p - C_p{}')}{36}\right)\right] \tag{17}$$

where $C_p{}'$ denotes the acoustic wave velocity after disturbance, unit = km/s.

4. NSCR Method for Slopes Based on the Hoek–Brown Criterion

4.1. Methodology

The basic parameters of the Hoek–Brown criterion can be determined using acoustic testing technology. Then, the equivalent cohesion and internal friction angle can be derived. This is followed by the introduction of the ARS, n, and the correlation factor, λ, to establish the relationship of coordination between cohesion and the internal friction angle in the strength reduction process. Finally, Comsol Multiphysics-6.0 finite element software is used for numerical calculation to establish an NSCR method based on the Hoek–Brown criterion.

4.2. Determination of the Equivalent Cohesion and Internal Friction Angle

GSI, *D*, m_b, s, and a can be determined via the acoustic wave velocity C_p before the disturbance, and the acoustic wave velocity $C_p{}'$ after the disturbance, which can be obtained by simultaneously solving the Equations (2)–(4), (10), and (17).

$$m_b = m_i \exp\left(\frac{13.64C_p{}' - 101.4}{28K}\right) \tag{18}$$

$$s = \exp\left(\frac{13.64C_p{}' - 101.4}{3 + 6K}\right) \tag{19}$$

$$a = \frac{1}{2} + \frac{1}{6}\left(e^{(1.4-13.64C_p{}')/15} - e^{-20/3}\right) \tag{20}$$

where $K = \exp\left(-13.64\left(C_p - C_p{}'\right)/36\right)$.

By combining Equations (11) and (17), the expression for the elastic modulus of the rock mass after disturbance can be obtained:

$$E_m = \begin{cases} K\sqrt{\frac{\sigma_c}{100}}10^{(13.64(C_p-C_p{}')-11.4)/40}(\sigma_c \le 100MPa) \\ K10^{(13.64(C_p-C_p{}')-11.4)/40}(\sigma_c \ge 100MPa) \end{cases} \tag{21}$$

Additionally, according to Hoek et al. [41], σ_{cm} and σ_{tm} can be determined and expressed as

$$\sigma_{cm} = \sigma_c \cdot s^a \tag{22}$$

$$\sigma_{tm} = -\sigma_c \cdot s / m_b \tag{23}$$

Using the nonlinear strength criterion linearization method [41,67], the equivalent cohesion (unit = MPa) and internal friction angle (unit = °) can be derived.

$$c = \frac{\sigma_c[(1+2a)s + (1-a)m_b\sigma_{3n}](s + m_b\sigma_{3n})^{a-1}}{2(1+a)(2+a)\sqrt{1 + \left(6am_b(s + m_b\sigma_{3n})^{a-1}\right)/((1+a)(2+a))}} \tag{24}$$

$$\phi = \sin^{-1}\left[\frac{6am_b(s + m_b\sigma_{3n})^{a-1}}{2(1+a)(2+a) + 6am_b(s + m_b\sigma_{3n})^{a-1}}\right] \tag{25}$$

where $\sigma_{3n} = \sigma_{3\max}/\sigma_c$.

In addition, for slopes, $\sigma_{3\max}$ can be expressed as

$$\frac{\sigma_{3\max}}{\sigma'_{cm}} = 0.72\left(\frac{\sigma'_{cm}}{\gamma H_s}\right)^{-0.91} \tag{26}$$

where γ denotes the bulk weight of the rock mass, and H_s is the height of the associated slope.

When $\sigma_{tm} < \sigma_3 < 0.25\sigma_c$, Hoek et al. suggest that σ'_{cm} can be expressed as

$$\sigma'_{cm} = \sigma_c \frac{[m_b + 4s - a(m_b - 8s)](m_b/4 + s)^{(a-1)}}{2(1+a)(2+a)} \tag{27}$$

Therefore, ultimately, all the parameters of the Hoek–Brown criterion and the compressive strength of the rock can be determined using the method of acoustic testing. This method is performed in order to determine the equivalent cohesion and the internal friction angle of the rock mass after disturbance, and to achieve the estimation of the mechanical parameters of the rock mass of the slope.

4.3. Principle of the NSCR Method

According to the actual deterioration mechanism of the rock [35] when the slope has a sliding tendency, if the cohesion is sufficient to resist the sliding force, the internal connecting bonds of the rock mass may not be broken; if the rock mass does not rotate in the shear direction, the friction resistance does not play a role. If the cohesion is insufficient to resist the sliding force, the internal connecting bonds of the rock mass may be partially or completely broken; if the rock mass rotates in the shear direction, friction resistance will play a role, and the degree of cohesion and the internal friction angle are different from the sequential order.

The idea of coordinated reduction considers that, in the process of slope destabilization, cohesion and internal friction angle play different roles and have different degrees of influence, possessing different reduction coefficients (i.e., double-reduction coefficients, respectively):

$$Fs_c = \frac{c_0}{c} \tag{28}$$

$$Fs_\varphi = \frac{\tan\varphi_0}{\tan\varphi} \tag{29}$$

When simulating the process of rock mass deterioration, it is assumed that the cohesion is reduced in advance, and the ARS is n; the interval size of the reduction coefficient (the accuracy of the safety factor) is m. Before the internal friction angle is reduced, the cohesion c is first reduced by a certain number of steps and then reduced to c'. The cohesion and internal friction angle are then reduced in a synchronous and coordinated manner. Referring to Xue et al. [34], it is assumed that the trend in the reduction of the double parameters is based on the linear softening model, which considers the strength parameter and the softening parameter to be piecewise linear functions. The softening parameter is set to η, and the strength parameter is the cohesion and the internal friction angle. The reduction model is shown in Figure 2.

Where c' is calculated as

$$c' = \frac{c}{1+nm} \tag{30}$$

When the ARS is $n = 0$, the synchronous coordinated reduction proposed by Xue et al. [34] is indicated.

From Figure 2, for the cohesive interval, the strength and softening parameters can be expressed as

$$c(\eta) = \begin{cases} c \ldots (\eta \le \eta_k) \\ \frac{c'-c}{\eta_p - \eta_k}(\eta - \eta_k) + c \ldots (\eta_k < \eta \le \eta_p) \\ \frac{c''-c'}{\eta_r - \eta_p}(\eta - \eta_p) + c' \ldots (\eta_p < \eta \le \eta_r) \\ c'' \ldots (\eta_k \le \eta) \end{cases} \tag{31}$$

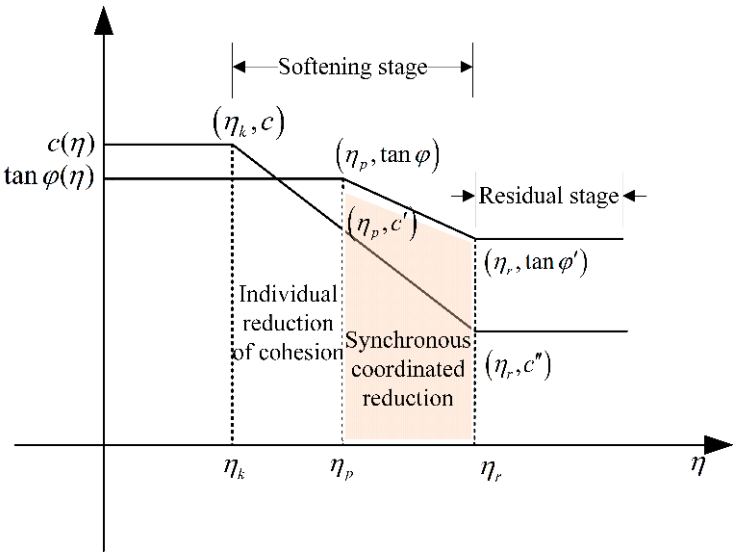


Figure 2. Schematic diagram of the NSCR method.

And for the internal friction angle

$$\tan\varphi(\eta) = \begin{cases} \tan\varphi \ldots (\eta \le \eta_p) \\ \frac{\tan\varphi' - \tan\varphi}{\eta_r - \eta_p}(\eta - \eta_p) + \tan\varphi \ldots (\eta_p < \eta \le \eta_r) \\ \tan\varphi' \ldots (\eta_r \le \eta) \end{cases} \tag{32}$$

From Equation (31), we can obtain

$$\frac{\eta - \eta_p}{\eta_r - \eta_p} = \frac{c(\eta) - c'}{c'' - c'} \tag{33}$$

Simultaneous Formulas (30) and (33):

$$\frac{\eta - \eta_p}{\eta_r - \eta_p} = \frac{c(\eta)(1 + nm) - c}{c''(1 + nm) - c} \tag{34}$$

From Equation (32), we can obtain

$$\frac{\eta - \eta_p}{\eta_r - \eta_p} = \frac{\tan\varphi(\eta) - \tan\varphi}{\tan\varphi' - \tan\varphi} \tag{35}$$

Simultaneous Formulas (34) and (35):

$$\frac{c(\eta)(1 + nm) - c}{c''(1 + nm) - c} = \frac{\tan\varphi(\eta) - \tan\varphi}{\tan\varphi' - \tan\varphi} \tag{36}$$

Equations (28) and (29) are then carried over to Equation (36) to obtain

$$\frac{c(\tan\varphi' - \tan\varphi)}{\tan\varphi\left(c''(1 + nm) - c\right)} = \frac{\left(\frac{1}{Fs_\varphi} - 1\right)}{\left(\frac{1}{Fs_c} - 1\right)} = \frac{(1 - Fs_\varphi)Fs_c}{(1 - Fs_c)Fs_\varphi} \tag{37}$$

Let $\lambda = \frac{c(\tan\varphi' - \tan\varphi)}{\tan\varphi\left(c''(1+nm) - c\right)}$; when $n = 0$, a case of synchronous coordinated reduction is indicated.

Then,

$$\lambda = \frac{(1 - Fs_\varphi)Fs_c}{(1 - Fs_c)Fs_\varphi} \tag{38}$$

Therefore, the reduction factor of the internal friction angle can be obtained from the reduction factor of the cohesion:

$$Fs_\varphi = \frac{Fs_c}{\lambda + (1 - \lambda)Fs_c} \tag{39}$$

or the reduction factor of the cohesion can be obtained from the reduction factor of the internal friction angle:

$$Fs_c = \frac{\lambda Fs_\varphi}{1 + (\lambda - 1)Fs_\varphi} \tag{40}$$

4.4. Determination of the CSF

When considering the respective reduction of the strength parameters of the slope, namely, cohesion and internal friction angle, two different reduction coefficients will be obtained, and the synthesis of the two reduction factors to obtain the final safety factor of the slope is the most important part of the process, considering the double-parameter reduction. Below is a summary of the current methodology for determining the CSF in the case of double-parameter coordinated reduction.

(1) When conducting double-parameter strength reduction, Tang et al. [30] proposed using the average reduction coefficients of cohesion and internal friction angle as the final CSF. Research has shown that the safety factor determined using this method is similar to the results obtained using the limit equilibrium method:

$$Fs = \left(Fs_c + Fs_\varphi\right)/2 \tag{41}$$

(2) W. Yuan et al. [32] conducted a study on numerous slope conditions, investigating the impact of slope weight, height, and angle on slope stability. They proposed a formula to calculate the overall safety factor during double-parameter reduction, which can be expressed as follows:

$$Fs = \left(\sqrt{2}Fs_cFs_\varphi\right)/\sqrt{{Fs_c}^2 + {Fs_\varphi}^2} \tag{42}$$

$$Fs = \sqrt{Fs_c \times Fs_\varphi} \tag{43}$$

(3) A. Isakov and Y. Moryachkov [33] proposed the Phi-c reduction method for determining the CSF through analysis of the minimum path of strength parameter reduction:

$$R = \sqrt{\left(1 - \frac{1}{Fs_c}\right)^2 + \left(1 - \frac{1}{Fs_\varphi}\right)^2} \tag{44}$$

$$Fs = 1/\left(1 - \frac{R}{\sqrt{2}}\right) \tag{45}$$

(4) Xue et al. [34] proposed a definition of the CSF taking into account the contribution of shear strength parameters to the anti-slip force; the weight and the physical meaning are relatively clear and can be expressed as

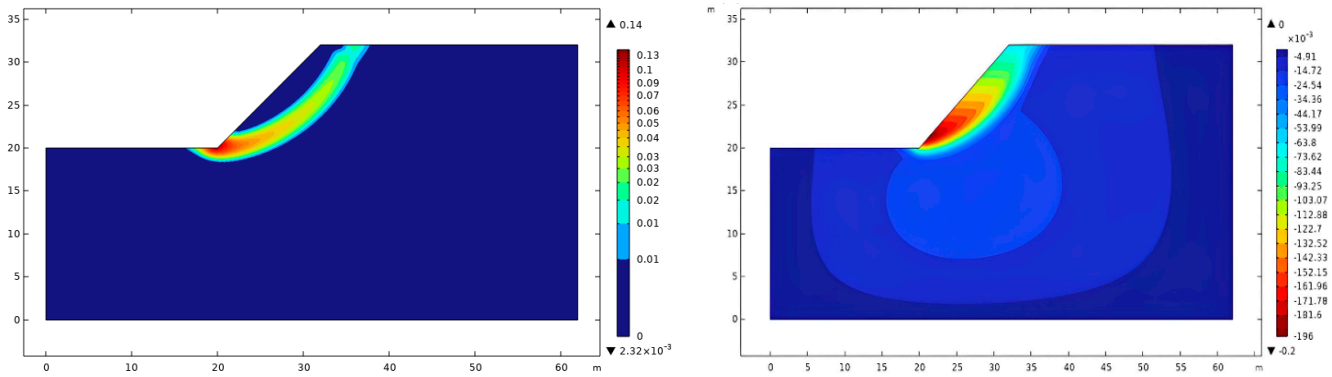
$$Fs = \omega_c Fs_c + \omega_\varphi Fs_\varphi = \frac{\int c_i ds}{\int \left(\frac{c_i}{Fs_c} + \sigma_i \frac{\tan\varphi_i}{Fs_\varphi}\right) ds} + \frac{\int \sigma_i \tan\varphi_i ds}{\int \left(\frac{c_i}{Fs_c} + \sigma_i \frac{\tan\varphi_i}{Fs_\varphi}\right) ds} \tag{46}$$

Considering the study slope [34], the slope height H = 12 m, the slope ratio is 1,1, and the parameters of the material are shown in Table 1.

Table 1. Slope material parameters.

Unit Weight/ (kN/m^3)	Poisson's Ratio	Elastic Modulus/ (MPa)	Peak Strength Parameters		Residual Strength Parameters	
			c/(KPa)	φ/(deg)	c'/(KPa)	φ'/(deg)
19.3	0.4	56.5	25	20	7.9	16.8

For the example slope, the double-parameter strength reduction method is used, combined with Com-sol-Multiphysics finite element software for slope strength reduction, and then the computation does not converge, the plastic strain region penetration as the slope instability criterion [31–34]; finally, the numerical calculation of the viscous cohesion reduction coefficient Fs_c produces a value of 1.78, and the internal friction angle reduction coefficient Fs_φ is 1.12. Figure 3 shows the equivalent plastic strain contour map and X-direction displacement cloud map, respectively, when the slope is destabilized. When the cohesion reduction coefficient Fs_c = 1.78, it is indicated that the plastic zone has been penetrated from the foot of the slope to the top of the slope. It can be observed that the very obvious plastic strain zone, i.e., the slope, is destabilized on the sliding surface. The maximum displacement in X direction is 0.2 m, and the maximum plastic strain is 0.14.



(**a**) (**b**)

Figure 3. Nephogram of plastic strain and displacement in the X−direction of the slope. (**a**) Equivalent plastic strain contour map of slope. (**b**) X−direction displacement cloud map of slope.

Comparing the calculation results of commonly used limit equilibrium methods such as the Morgenstern–Price method and Bishop's method (in which the force function between the bars of the Morgenstern–Price method is set as half-sinusoidal), the different CSFs are shown in Table 2. Based on Table 2, it can be seen that the CSF calculated according to W. Yuan is closer to the limit equilibrium method and has the smallest safety factor. When compared to the limit equilibrium method, the other integrated methods produce a larger safety factor and have a relatively large error; the maximum error reaches 0.117.

Table 2. Comparison of safety factors between the limit equilibrium method and coordinated reduction method.

Limit Equilibrium Method		Coordinated Reduction Method				
M-Price	Bishop	Tang et al. [30]	W. Yuan-1 [32]	W. Yuan-2 [32]	A. Isakov et al. [33]	Xue et al. [34]
1.352	1.354	1.451	1.343	1.416	1.469	1.377

Note: W. Yuan-1 represents the CSF calculated according to Equation (42), and W. Yuan-2 represents the CSF calculated according to Equation (43).

5. Examples of NSCR Application in Slope Stability Analysis

5.1. Field Experiments of Acoustic Testing

The diabase mine at Yanshi Quarry is located in Maojian District, Shiyan City, Hubei Province, China. The mining area covers an area of 0.0591 square kilometers and is situated in a region with a subtropical humid monsoon climate. The annual average temperature is approximately 15.5 °C, with extreme highs of 41.1 °C and extreme lows of −14.9 °C. The average annual rainfall is 828.5 mm. The mining area is located at the junction between low mountain slopes and hilly areas, characterized by strong surface cutting and the development of valleys. The geological structure and lithology in the mining area are relatively simple, with the main mineral component being Jinning Period Diabase (βμ). The rock fractures are not well developed, and most are in a closed state.

The blasting parameters in the quarry are as follows: the hole spacing is 3–4 m, the row spacing is 2.5–3 m, the individual hole charge is approximately 35 kg, and the total charge per blasting is approximately 100 kg. To avoid overlapping waveforms between sections, a millisecond delay blasting technique is employed, with five sections of millisecond detonating tubes inside the holes and seven sections outside the holes. Strict control of the blasting parameters in the quarry ensures consistent blasting scales, resulting in comparable acoustic testing data after each blasting. With the increasing depth of excavation, the quarry forms a steep artificial slope of approximately 60 m, with a slope angle of approximately 60°.

Using an acoustic testing method and a cross-hole testing method, we carried out a field test on the formed slope. At 1.2 m from the foot of the slope, two groups of four acoustic test holes were drilled; the acoustic test holes were numbered 1 #, 2 #, 3 #, and 4 #. Holes 1 # and 2 # made up the first group, and 3 # and 4 # made up the second group. Each group of acoustic test holes had 1.1 m spacing, a hole diameter of 90 mm, and a hole depth of 5.75 m. The acoustic test holes were tilted downward by 10 °, making water storage easy, as shown in Figure 4.

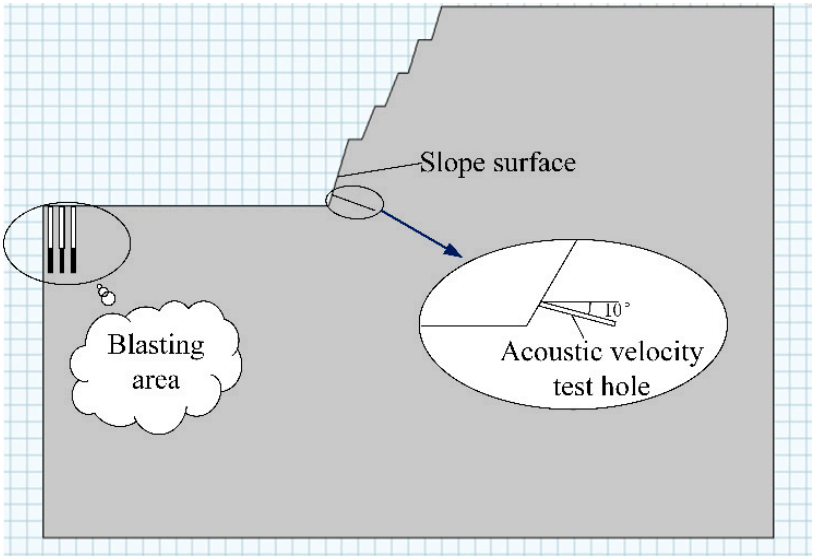
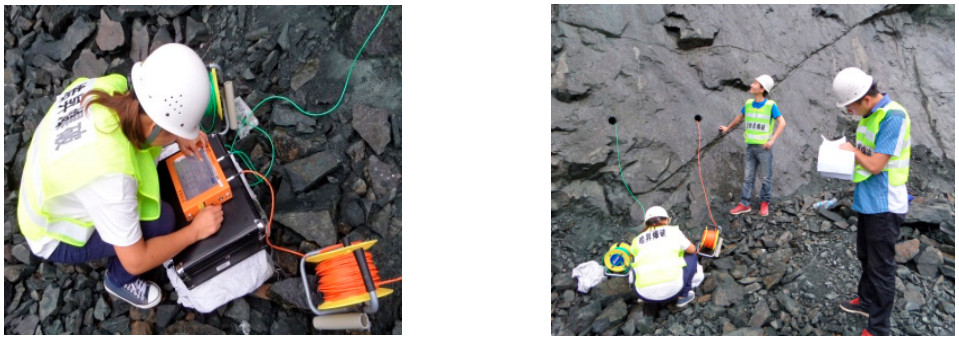


Figure 4. Hole design for acoustic wave testing on the steep slope.

During the test, readings were taken at 25 cm intervals, and the same measurement point was measured twice, while the average value was taken as the final acoustic wave velocity value; for the anomalous measurement point, readings were taken three times, and the difference in readings was controlled at less than 5%. The average of the two closest measurements was taken as the acoustic wave velocity value. In order to avoid reading errors, the method of automatic reading was adopted (Figure 5).



(**a**) (**b**)

Figure 5. Acoustic testing site. (**a**) Modulation instrument. (**b**) Acoustic wave velocity detection.

5.2. Determination of Mechanical Parameters of Slope Rocks

The slope parameters were assessed under multiple blast disturbances, taking the average value of acoustic wave velocity at different depths of the first blast as the initial acoustic wave velocity (non-disturbed case). The average value of the acoustic wave velocity at different depths of the last blast was taken as the disturbed acoustic wave velocity, and the changing trend in the acoustic wave velocity with a different number of blasts is shown in Figure 6.

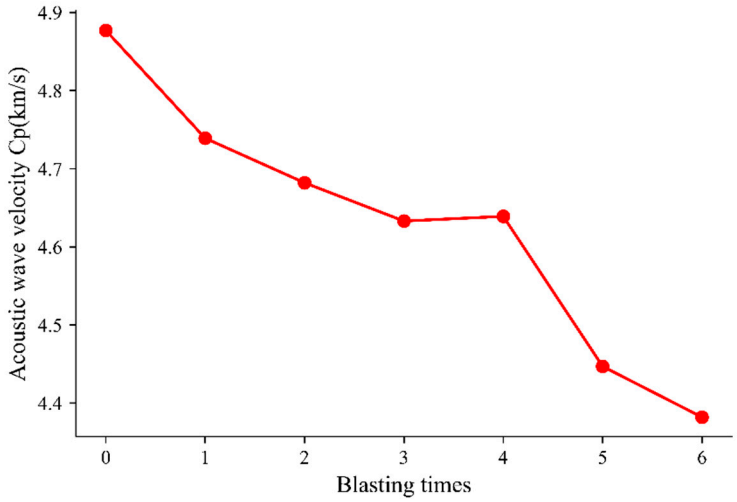


Figure 6. Variation trend in acoustic wave velocity with different blasting times of rock mass.

The effective wave velocities, C_p and C_p', of the slope body (obtained from Figure 6) are 4.8774 km/s and 4.3818 km/s, respectively. The geological strength index (*GSI*) of the slope rock mass after disturbance, obtained using Equations (10) and (17), is 58. Additionally, the disturbance factor (*D*) is 0.35. The elastic modulus (E_m) of the diabase after the slope disturbance is determined to be 13.38×10^9 Pa, using Equation (11) and considering the rock mechanical parameters from the engineering geology manual and the geological survey data. Moreover, the Poisson's ratio (μ) is 0.135, the density (ρ) is 2800 kg/m^3, and the stresses (σ_c and σ_t) are 20 MPa and 1.5 MPa, respectively. The parameters after perturbation, mi, mb, s, and a, can be calculated as 13.3, 2.153, 0.005, and 0.503, respectively, using Equations (18)–(20). The height of the adjacent slope is 60 m, and the slope angle is approximately 60°, calculated using Equations (24) and (25). The equivalent cohesion and internal friction angles of the slope rock mass after the blasting disturbance are determined to be 0.89 MPa and 21.77°, respectively. Furthermore, the relevant parameters of the slope rock mass before the blasting disturbance are calculated and presented in Table 3.

Table 3. Parameters determined using the acoustic test method.

Rock Mass State	*GSI*	D	m_i	m_b	s	a	*c*/MPa	φ/°
Before blasting	65.16	0	13.33	3.74	0.02	0.50	1.05	25.68
After blasting	58.34	0.35	13.33	2.15	0.005	0.50	0.89	21.77

From Table 3, it can be seen that the strength of the rock body is significantly reduced by multiple blast disturbances, and the equivalent cohesion of the rock body decreases from 1.05 MPa to 0.89 MPa, while the internal friction angle of the rock body decreases from 25.68° to 21.77°; blast disturbances are one of the most important factors in the deterioration of the strength of the rock body. As there are numerous formulas, this paper uses a GUI written in Python language to improve the efficiency of calculation.

5.3. Numerical Calculations

5.3.1. Slope NSCR Method Process and Parameter Setting

Comsol Multiphysics finite element software has a very good simulation effect in the field of multi-physics modeling as well as advanced numerical simulation; it is widely used in various fields of scientific research and engineering calculations [67,68]. It is also applied in geotechnical engineering and slope stability analysis [69–73] and has obtained very good results. This study focuses on computational research into NSCR using Comsol Multiphysics finite element software. The specific numerical calculation process is as follows:

(1) The material parameters of the slope are set, and the geometric model of the slope is established.

(2) Two variables are created in the definition module to define the cohesion and the reduction factor for the internal friction angle, respectively, so that the cohesion factor is equal to *Fs*. The cohesion is reduced in advance to $c' = \frac{c}{1+nm}$. Additionally, the cohesion, which reduces synchronously with the internal friction angle, is defined as $c'' = \frac{c'}{Fs}$. Moreover, the reduction factor for the internal friction angle, F_φ, is calculated using Equation (39), where $\lambda = \frac{c(\tan\varphi' - \tan\varphi)}{\tan\varphi\left(c''(1+nm)-c\right)}$ is defined in advance in the material module, so the reduced internal friction angle is defined as $\varphi' = \arctan(\frac{\tan(\varphi)}{F_\varphi})$.

(3) The slope is defined as an elastic–plastic model, and the damage criterion is set as the Mohr–Coulomb criterion; then, the material parameters are filled in.

(4) The slope model is meshed, and the stress conditions and boundary conditions of the slope are set.

(5) The calculation study type is set to steady-state; the auxiliary sweep is selected within the study extension; the reduction factor Fs is selected for the parameter; the range is set (1,15); and the accuracy is set to 0.02. Then, based on the calculation of non-convergence, the plastic zone penetrates from the foot of the slope to the top of the slope, and the reduction coefficient at this time is determined as the reduction coefficient $Fs = Fs_c$ of the cohesion. Then, the reduction coefficient of the internal friction angle can be obtained using the Formula (39); finally, the ultimate safety factor of the slope is obtained using the CSF method.

5.3.2. Numerical Calculation Models

After the research and calculation in the previous chapter, the mechanical parameters of the rock mass before and after the blasting disturbance were estimated. Because the influence of Poisson's ratio on the stability of the slope was negligible [74], it was not calculated and discussed; the height of the multi-level slope is 60 m, and the slope angle is about 60°. The specific geometric model is shown in Figure 7.

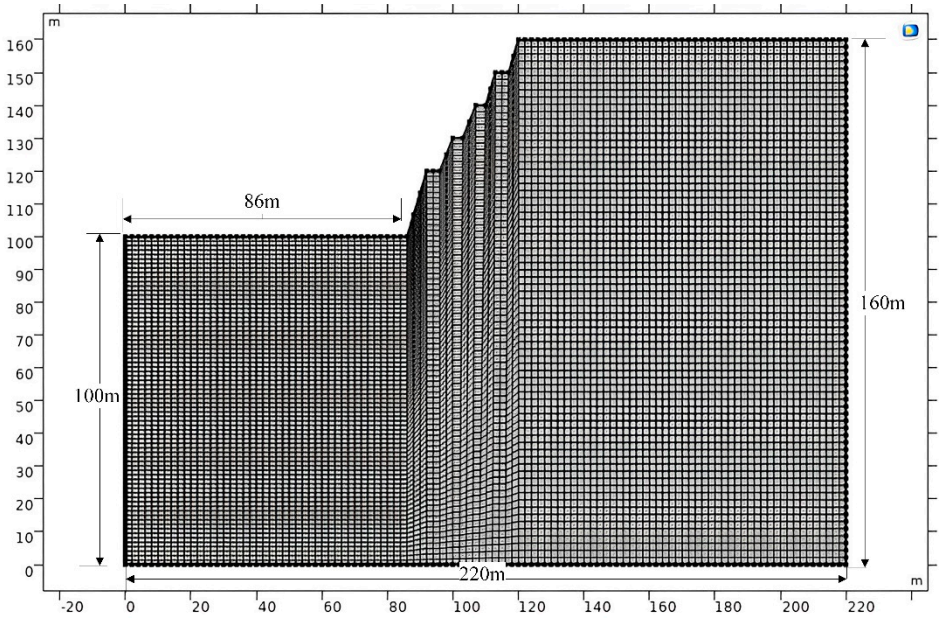


Figure 7. Geometric model of the slope.

5.4. Analysis and Discussion of Results

In order to properly simulate the slope stability after the blasting disturbance, the reduction in the cohesion and internal friction angle follow the actual deterioration law of the rock mass, i.e., the paths of the weakening phase are calculated with reference to the cohesion and internal friction angle before and after the disturbance so as to determine the correlation relationship. At this time, the strength parameters of the rock slope are as follows: the cohesion is 0.89 MPa, the internal friction angle is 21.77°, the residual strength/cohesion is 0.02 MPa, and the internal friction angle is 18.16°. Then, $\lambda = \frac{c(\tan\varphi' - \tan\varphi)}{\tan\varphi\left(c'(1+nm)-c\right)}$ is applied. First, taking $n = 0$ and $m = 0.02$, the default first synchronized coordinated reduction yields $\lambda = 0.19$, Therefore, the correlation between the cohesion reduction factor Fs_c and the internal friction angle reduction factor Fs_φ can be determined. Specifically, Fs_φ is calculated from Equation (39),

$$Fs_\varphi = \frac{Fs_c}{0.19 + (1 - 0.19)Fs_c}$$

Then, the cases of n = 50, 75, 100, 125, 150, and 175 were taken to simulate the NSCR of cohesion and the internal friction angle.

However, when compared with the calculation results of the limit equilibrium method, it is evident that the safety factor calculated using the traditional strength reduction method is 4.71, whereas the safety factor calculated using the limit equilibrium method (taking the Bishop method as an example) is 3.43. The difference between the values is significant, with an absolute error of 1.28. Meanwhile, when performing the calculation of equal reduction, the reduction path curve of the cohesion and the internal friction angle is obtained, as shown in Figure 8. The cohesion is reduced from 0.89 MPa to 0.19 MPa, and the internal friction angle is reduced from 21.77° to 4.84° until the slope fails and becomes unstable and damaged. Moreover, the internal friction angle is reduced to 4.84° at this point, thereby exceeding the limit value of the residual strength of the internal friction angle and going against the actual deterioration law of the rock mass. Therefore, the traditional strength reduction method is not suitable for analyzing the stability of rock slopes.

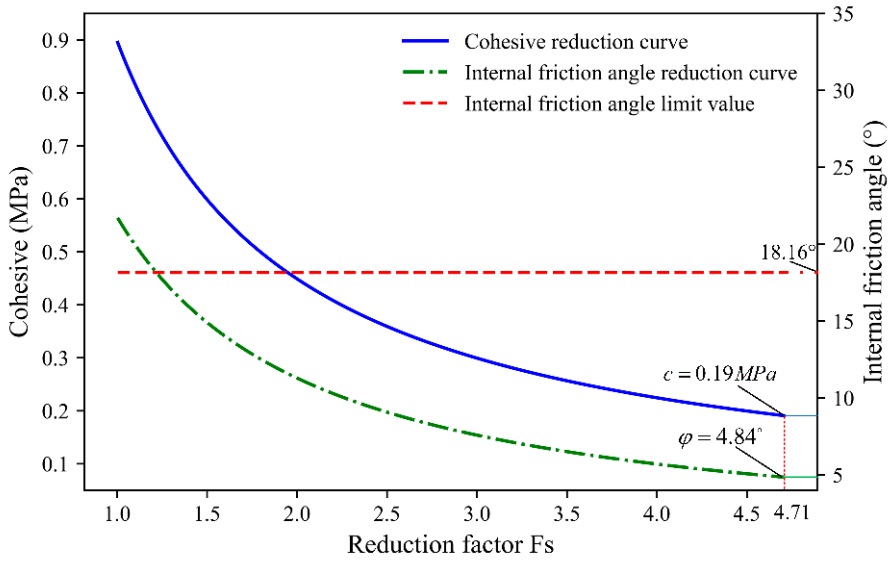


Figure 8. Reduction path curves of cohesion and internal friction angle undergoing equal reduction.

Therefore, it is more reasonable to calculate the safety factors of double-parameter coordinated reduction according to the actual deterioration path of the rock mass. First of all, when $n = 0$, this value indicates that the cohesion and internal friction angle undergo synchronously coordinated reductions. This is an example of Xue et al.'s non-equal coordinated reduction method. The reduction path curve of cohesion and the internal friction angle is shown in Figure 9.

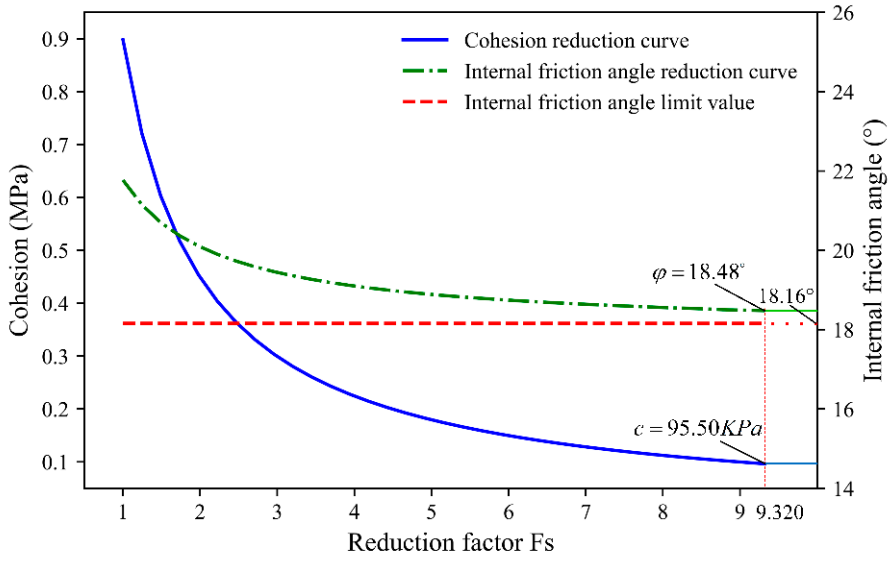


Figure 9. Reduction path curves of cohesion and internal friction angle undergoing non-equal coordinated reduction.

At this time, the path of double-parameter reduction is completely in accordance with the path of the rock mass strength parameter to the residual parameter, and the double parameter has its own reduction coefficient; when the slope is unstable and broken, the calculation does not converge, and the plastic zone fully penetrates to the top of the slope. The reduction coefficient Fs_c of the cohesion is 9.320, the reduction coefficient of internal friction angle Fs_φ is 1.195, and the cohesion and internal friction angles are 95.50 KPa and 18.48°, respectively. The results of the comprehensive method calculation are shown in Table 4.

Table 4. CSF calculated using different non-equal coordinated reduction methods.

Fs	Limit Equilibrium Method	CSF				
	Bishop	**Tang et al. [30]**	**W. Yuan-1 [32]**	**W. Yuan-2 [32]**	**A. Isakov et al. [33]**	**Xue et al. [34]**
	3.43	**5.25**	**1.67**	**3.33**	**2.79**	**2.16**
Error compared to the limit equilibrium method	0	1.82	1.75	0.09	0.63	1.26

Based on Table 4, we observed that the method of calculating CSF using averages is not suitable for the calculation of the stability safety factor of rock slopes, and the error reaches a maximum of 1.82. The CSF calculation method involving W. Yuan-2 and the A. Isakov method is similar to the limit equilibrium method in that the relative error between the result of the W. Yuan-2 method and the result of the limit equilibrium method is only 9%, making it suitable for the calculation of the double-parameter coordinated reduction of slope stability.

When the ARS n = 50, the cohesion is reduced to 0.445 MPa in advance, and then the cohesion and internal friction angle undergo synchronously coordinated reduction. The reduction path curve of the cohesion and internal friction angle is shown in Figure 10.

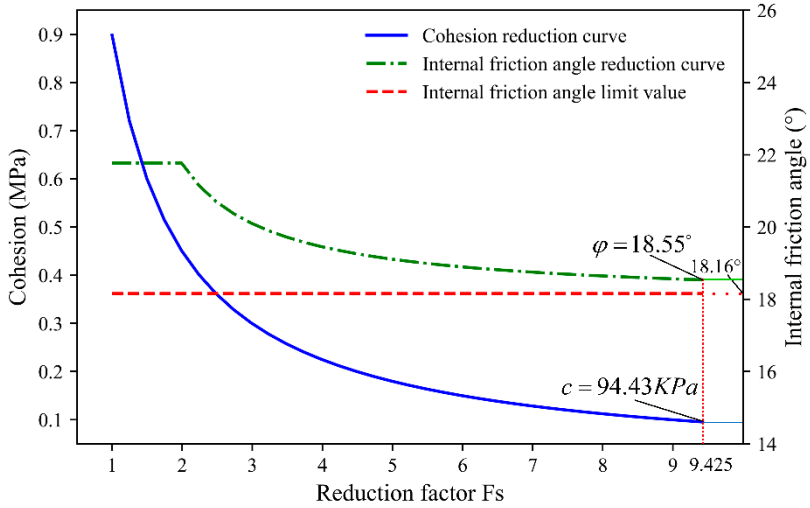


Figure 10. Reduction path curves of cohesion and internal friction angle under the conditions of NSCR when n = 50.

In the process of NSCR, in observing the equivalent plastic strain contour map, we can see the process of the gradual failure of the slope. The plastic zone of the slope is first formed at the foot of the slope (Figure 11a); then, with the increase in the reduction coefficient, the plastic zone of the slope gradually extends from the foot to the top of the slope (Figure 11b,c) until it is completely penetrated (Figure 11d). Finally, the software will prompt that the calculation does not converge until the end of the calculation, the process of which is shown in Figure 11.

When the slope is unstable and broken, the reduction coefficient Fs_c of the cohesion is 9.425; the reduction coefficient of the internal friction angle Fs_φ is 1.190; the cohesion and internal friction angles are 94.43 Kpa and 18.55°, respectively; and the CSF values determined using different methods are shown in Table 5. It can be seen from Table 5 that different CSF determination methods have a great influence on the final slope safety factor. The CSF obtained using the Yuan-2 calculation method is the closest to that of the limit equilibrium method, with a relative error of only 8.1%.

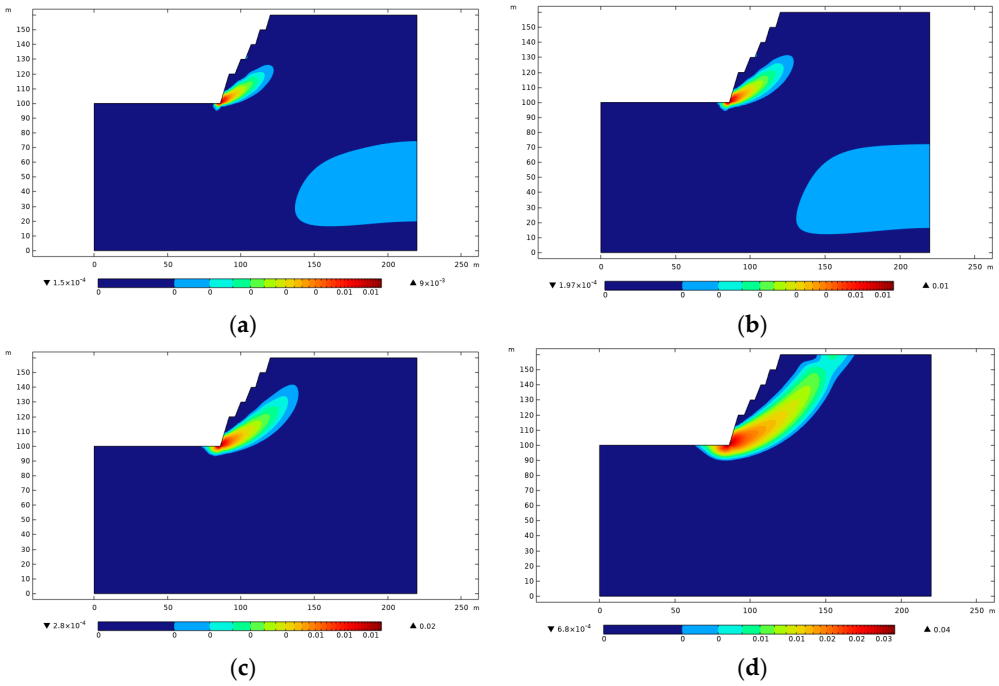


Figure 11. Nephogram of the slope's plastic strain as affected by different reduction factors. (**a**) Fs_c = 8.82. (**b**) Fs_c = 9.02. (**c**) Fs_c = 9.22. (**d**) Fs_c = 9.425.

Table 5. CSF calculated using different methods when n = 50.

Fs	Limit Equilibrium Method	CSF				
	Bishop	**Tang et al. [30]**	**W. Yuan-1 [32]**	**W. Yuan-2 [32]**	**A. Isakov et al. [33]**	**Xue et al. [34]**
	3.43	**5.30**	**1.67**	**3.35**	**2.79**	**2.17**
Error compared to the limit equilibrium method	0	1.87	1.76	0.081	0.63	1.26

Using the comprehensive method of W. Yuan-2, we were able to calculate the CSF when n = 75, 100, 125, 150, and 175, sequentially. The obtained cohesion reduction coefficients Fs_c are 9.431, 9.435, 9.441, 9.446, and 9.443, and the internal friction angle reduction coefficients Fs_φ are 1.187, 1.185, 1.183, 1.180, and 1.178, respectively. The CSF values, as affected by different n values, are shown in Table 6.

Table 6. CSF values affected by different n values.

The Value of *n*	***n* = 0**	***n* = 50**	***n* = 75**	***n* = 100**	***n* = 125**	***n* = 150**	***n* = 175**
Fs	3.337	3.349	3.346	3.344	3.342	3.338	3.335
Error compared to the limit equilibrium method	0.093	0.081	0.084	0.086	0.088	0.092	0.095

It can be seen from Table 6 that with the increase in the number of steps n in advance, the CSF shows a trend of increasing first and then decreasing, and the relative error within the results calculated using the limit equilibrium method is less than 10%. The safety factor at n = 50 is closer to the result of the limit equilibrium method, indicating that it is feasible to adopt the NSCR method for rock slopes. At the same time, this method establishes an NSCR relationship between the cohesion reduction coefficient and

the internal friction angle reduction coefficient, and in the process of the double-strength reduction, the reduction coefficient of the internal friction angle will change with the change in the viscosity reduction coefficient; thus, the determination of the double-reduction coefficient becomes the determination of a single-reduction coefficient, thereby overcoming the blindness of the proportional relationship between the cohesion and internal friction angle reduction coefficients assumed due to the existing double-reduction coefficient method, and can be reduced according to the law of the actual deterioration of the rock mass. The relationship between the reduction of material parameters and the deterioration of real material properties is considered to ensure that the reduction interval of the internal friction angle is not lower than the limit value of the residual strength. Other reduction methods often do not depend on the real parameters of the material and are divorced from reality; on the contrary, the double safety factor obtained through the NSCR method makes it more convincing.

6. Conclusions

In this paper, the parameters of the slope rock mass are preliminarily estimated via acoustic testing, and a double-parameter NSCR method for rock slopes is proposed; the practical feasibility of this method is verified using application examples. The following conclusions were reached:

Different CSF calculation methods have a great influence on the final slope safety factor; the CSF of the slope calculated using the Yuan-2 method is closer to the value reached with the limit equilibrium method, making it suitable for the calculation of the safety factors of the double-parameter coordinated reduction.

The acoustic test method can better estimate the parameters of the slope rock mass, and the strength index of the slope rock mass is significantly reduced after multiple blasting disturbances. The equivalent cohesion of the rock mass is reduced from 1.05 MPa to 0.89 MPa, and the internal friction angle of the rock mass is reduced from 25.68° to 21.77°.

In the calculation process of proportional strength reduction, the cohesion of the rock mass is reduced from 0.89 MPa to 0.19 MPa, and the internal friction angle is reduced from 21.77° to 4.84°, thereby exceeding the limit value of the residual strength of the internal friction angle and violating the actual deterioration law of the slope rock mass.

In the calculation process of the NSCR of a slope, the CSF of the slope shows a trend of first increasing and then decreasing with the increase in n. F_S = 3.349 when n = 50, with a relative error of only 8.1% compared to the results calculated using the limit equilibrium method. The NSCR method establishes a correlation between double parameters through practical expressions and considers the order of decrement in these parameters. It remediates the issue of blindness in traditional strength reduction methods through decrementing double parameters and ensures that the range of the reduction in the internal friction angle is no lower than its remaining strength limit. This method has proved to be practical and feasible for the analysis of slope stability.

Author Contributions: Conceptualization, Y.Z.; methodology, Y.Z.; equipment, D.Z. and L.H.; validation, L.H. and D.Z.; formal analysis, L.H. and Y.Z.; investigation, L.H., Y.Z. and H.X.; resources, L.H. and D.Z.; data curation, L.H., D.Z. and Y.Z.; writing—original draft preparation, Y.Z.; writing—review and editing, L.H.; visualization, L.H.; translation, L.H., Y.Z., L.Y., S.C. and X.Z.; supervision, D.Z.; project administration, L.H. and D.Z.; funding acquisition, L.H. All authors have read and agreed to the published version of the manuscript.

Funding: This study was supported by the National Natural Science Foundation of China (grant nos. 52274136 and 51904210); the Foundation Project of Hubei Key Laboratory of Blasting Engineering (grant no. BL2021-11), and the Key R&D Project of Hubei Province (grant no. 2020BCA084).

Institutional Review Board Statement: Not applicable.

Data Availability Statement: Not applicable.

Conflicts of Interest: The authors declare no conflict of interest.

References

1. Dong, M.; Zhang, F.; Yu, C.; Lv, J.; Zhou, H.; Li, Y.; Zhong, Y. Influence of a Dominant Fault on the Deformation and Failure Mode of Anti-dip Layered Rock Slopes. *KSCE J. Civ. Eng.* **2022**, *26*, 3430–3439.
2. Li, D.; Sun, M.; Yan, E.; Yang, T. The Effects of Seismic Coefficient Uncertainty on Pseudo-Static Slope Stability: A Probabilistic Sensitivity Analysis. *Sustainability* **2021**, *13*, 8647.
3. Song, D.; Quan, X.; Liu, M.; Liu, C.; Liu, W.; Wang, X.; Han, D. Investigation on the Seismic Wave Propagation Characteristics Excited by Explosion Source in High-Steep Rock Slope Site Using Discrete Element Method. *Sustainability* **2022**, *14*, 17028.
4. Komadja, G.C.; Rana, A.; Glodji, L.A.; Anye, V.; Jadaun, G.; Onwualu, P.A.; Sawmliana, C. Assessing Ground Vibration Caused by Rock Blasting in Surface Mines Using Machine-Learning Approaches: A Comparison of CART, SVR and MARS. *Sustainability* **2022**, *14*, 11060.
5. Wang, Y.; Zheng, G.; Li, Y.; Zhang, F. Full Waveform Prediction of Blasting Vibration Using Deep Learning. *Sustainability* **2022**, *14*, 8200. [CrossRef]
6. He, L.; Zhong, D.; Liu, Y.; Song, K. Prediction of bench blasting vibration on slope and safety threshold of blasting vibration velocity to undercrossing tunnel. *Shock. Vib.* **2021**, *2021*, 9939361. [CrossRef]
7. Wang, H.; Zhao, Y.; Shan, R.; Wei, Y.; Liu, D.; Dong, J. Safety Evaluation and Application of Blasting Vibration Based on an Improved Hilbert–Huang Transform. *Rock Mech. Rock Eng.* **2023**, *56*, 3971–3991.
8. Nie, W.; Wang, W.Q.; Tao, Z.G.; Chen, Y.; Zhu, C. Numerical modeling of the NPR-cable and its applications for analysis of a slide-toe-toppling failure. *Comput. Geotech.* **2022**, *149*, 104852.
9. Dong, M.; Zhang, F.; Hu, M.; Liu, C. Study on the Influence of Anchorage Angle on the Anchorage Effect of Soft-hard Interbedded Toppling Deformed Rock Mass. *KSCE J. Civ. Eng.* **2020**, *24*, 2382–2392.
10. Azarafza, M.; Akgün, H.; Ghazifard, A.; Asghari-Kaljahi, E.; Rahnamarad, J.; Derakhshani, R. Discontinuous rock slope stability analysis by limit equilibrium approaches a review. *Int. J. Digit. Earth* **2021**, *14*, 1918–1941.
11. Deng, D. Limit equilibrium analysis on the stability of rock wedges with linear and nonlinear strength criteria. *Int. J. Rock Mech. Min. Sci.* **2021**, *148*, 104967.
12. Song, J.; Lu, Z.; Xie, H.; Zhang, F.; Ji, J.; Gao, Y. Coupled slip analysis of shallow and deep seismic slope based on limit equilibrium principle. *J. Geotech. Eng.* **2023**, *45*, 1141–1150.
13. Yang, Y.; Zhou, W.; Jiskani, I.M.; Lu, X.; Wang, Z.; Luan, B. Slope Stability Prediction Method Based on Intelligent Optimization and Machine Learning Algorithms. *Sustainability* **2023**, *15*, 1169.
14. Pham, B.T.; Qi, C.; Ho, L.S.; Nguyen-Thoi, T.; Al-Ansari, N.; Nguyen, M.D.; Nguyen, H.D.; Ly, H.-B.; Le, H.V.; Prakash, I. A Novel Hybrid Soft Computing Model Using Random Forest and Particle Swarm Optimization for Estimation of Undrained Shear Strength of Soil. *Sustainability* **2020**, *12*, 2218. [CrossRef]
15. Liu, S.; Shao, L.; Li, H. Slope stability analysis using the limit equilibrium method and two finite element methods. *Comput. Geotech.* **2015**, *63*, 291–298.
16. Shao, L.; Wang, H.; Jiang, Z. Stability analysis of Geotechnical structures based on finite element limit equilibrium method. *China Min. Mag.* **2021**, *30*, 170–177.
17. Zienkiewicz, O.C.; Humpheson, C.; Lewis, R.W. Discussion: Associated and non-associated viscoplasticity and plasticity in soil mechanics. *Geotechnique* **1977**, *27*, 101–102. [CrossRef]
18. Nguyen-Xuan, H.; Nguyen-Hoang, S.; Rabczuk, T.; Hackl, K. A polytree-based adaptive approach to limit analysis of cracked structures. *Comput. Methods Appl. Mech. Eng.* **2017**, *313*, 1006–1039.
19. Sun, L.; Liu, Q.; Abdelaziz, A.; Tang, X.; Grasselli, G. Simulating the entire progressive failure process of rock slopes using the combined finite-discrete element method. *Comput. Geotech.* **2022**, *141*, 104557. [CrossRef]
20. Wang, J.; Liu, P.; Si, P.; Li, H.; Wu, F.; Su, Y.; Long, Y.; Cao, A.; Sun, Y.; Zhang, Q. Three-Dimensional Stability Analysis of Ridge Slope Using Strength Reduction Method Based on Unified Strength Criterion. *Appl. Sci.* **2023**, *13*, 1580. [CrossRef]
21. Kumar, S.; Choudhary, S.S.; Burman, A. Recent advances in 3D slope stability analysis: A detailed review. *Model. Earth Syst. Environ.* **2023**, *9*, 1445–1462. [CrossRef]
22. Tao, Z.; Geng, Q.; Zhu, C.; He, M.; Cai, H.; Pang, S.; Meng, X. The mechanical mechanism of large-scale toppling failure for counter-inclined rock slopes. *J. Geophys. Eng.* **2019**, *16*, 541–558.
23. Xu, Z.; Chen, G.; Sun, X.; Yang, X.; Lin, Z. Method for Unloading Zonation Based on Strain per Unit Crack: Case Study of a Large-Scale Rocky Slope on the Qinghai–Tibet Plateau. *Sustainability* **2023**, *15*, 3861. [CrossRef]
24. Liu, Y. Non-proportional correlation asynchronous strength reduction method for loess slope stability by finite element method. Master's Thesis, Xi'an University of Technology, Xi'an, China, 2020.
25. Guo, S.; Li, N.; Liu, C.; Liu, N.; Liu, W. Unraveling the Progressive Failure Behaviors and Mechanisms of the Slope with a Local Dynamic Method Based on the Double Strength Reduction. *Int. J. Geomech.* **2020**, *20*, 04020069. [CrossRef]
26. Zou, J.; Yang, F.; Yuan, W.; Liu, Y.; Liu, A.; Wei, Z. A kinetic energy-based failure criterion for defining slope stability by PFEM strength reduction. *Eng. Fail. Anal.* **2023**, *145*, 107040. [CrossRef]
27. Taylor, D.W. *Fundamentals of Soil Mechanics*; John Wiley and Sons: New York, NY, USA, 1948.
28. Barton, N.; Pandey, S.K. Numerical modelling of two stoping methods in two Indian mines using degradation of c and mobilization of φ based on Q-parameters. *Int. J. Rock Mech. Min. Sci.* **2011**, *48*, 1095–1112. [CrossRef]

29. Guo, M.; Ge, X.; Wang, S.; Wang, H. Dynamic stability analysis of slope based on vector sum method. *J. Rock Mech. Eng.* **2011**, *30*, 572–579.
30. Tang, F.; Zheng, Y.; Zhao, S. Discussion on double safety factors of progressive failure of soil slope. *J. Rock Mech. Eng.* **2007**, *26*, 1402–1407.
31. Jiang, X.; Wang, Z.; Liu, L.; Zhou, Z. The determination of reduction ratio factor in homogeneous soil-slope with finite element double strength reduction method. *Open Civ. Eng. J.* **2013**, *7*, 205–209. [CrossRef]
32. Yuan, W.; Bai, B.; Li, X.; Wang, H.B. A strength reduction method based on double reduction parameters and its application. *J. Cent. South Univ.* **2013**, *20*, 2555–2562. [CrossRef]
33. Isakov, A.; Moryachkov, Y. Estimation of slope stability using two-parameter criterion of stability. *Int. J. Geomech.* **2014**, *14*, 06014004. [CrossRef]
34. Xue, H.; Dang, F.N.; Ying, X.T.; Yang, C.; Yan, F. Study on non-proportional correlation reduction method of slope strength parameters. *J. Rock Mech. Eng.* **2015**, *34*, 4005–4012.
35. Terzaghi, K.; Peck, R.B.; Mesri, G. Soil Mechanics in Engineering Practice. John Wiley & Sons: Hoboken, NJ, USA, 1996.
36. Chen, G.-Q.; Huang, R.-Q.; Xu, Q.; Li, T.-B.; Zhu, M.-L. Progressive modelling of the gravity-induced landslide using the local dynamic strength reduction method. *J. Mt. Sci.* **2013**, *10*, 532–540. [CrossRef]
37. Wang, Y.; Zhang, N.; Wu, W.; Cao, J.; Guo, Y.; Duan, D. Damage Data Analysis of Deep Coal Roadway Roof and Application of Long Anchorage and Zone Linkage Support Technology. *Sustainability* **2022**, *14*, 8092. [CrossRef]
38. Que, X.; Zhu, Z.; He, Y.; Niu, Z.; Huang, H. Strength and deformation characteristics of irregular columnar jointed rock mass: A combined experimental and theoretical study. *J. Rock Mech. Geotech. Eng. Engl. Ed.* **2023**, *15*, 429–441. [CrossRef]
39. Hossein, R.R.; Ming, C. Forty-Year Review of the Hoek–Brown Failure Criterion for Jointed Rock Masses. *Rock Mech. Rock Eng.* **2022**, *55*, 439–461.
40. Karrech, A.; Dong, X.; Elchalakani, M.; Basarir, H.; Shahin, M.A.; Regenauer-Lieb, K. Limit analysis for the seismic stability of three-dimensional rock slopes using the generalized Hoek-Brown criterion ScienceDirect. *Int. J. Min. Sci. Technol.* **2022**, *32*, 237–245. [CrossRef]
41. Hoek, E.; Marinos, P.; Benissi, M. Applicability of the Geological Strength Index (GSI) classification for very weak and sheared rock masses. The case of the Athens Schist Formation. *Bull. Eng. Geol. Environ.* **1998**, *57*, 151–160. [CrossRef]
42. Hoek, E.; Carranza-Torres, C.; Corkum, B. Hoek-Brown failure criterion-2002 edition. *Proc. NARMS-Tac* **2002**, *1*, 267–273.
43. Zhang, Z.L.; Xu, W.J.; Xia, W.; Zhang, H.Y. Large-scale in-situ test for mechanical characterization of soil–rock mixture used in an embankment dam. *Int. J. Rock Mech. Min. Sci.* **2016**, *86*, 317–322. [CrossRef]
44. Feng, W.; Dong, S.; Wang, Q.; Yi, X.; Liu, Z.; Bai, H. Improving the Hoek–Brown criterion based on the disturbance factor and geological strength index quantification. *Int. J. Rock Mech. Min. Sci.* **2018**, *108*, 96–104. [CrossRef]
45. Li, J.; Lian, S.; Huang, Y.; Wang, C. Study on Crack Classification Criterion and Failure Evaluation Index of Red Sandstone Based on Acoustic Emission Parameter Analysis. *Sustainability* **2022**, *14*, 5143. [CrossRef]
46. Dong, L.; Chen, J.; Song, D.; Wang, C.; Liu, X.; Liu, M.; Wang, E. Application of Long-Range Cross-Hole Acoustic Wave Detection Technology in Geotechnical Engineering Detection: Case Studies of Tunnel-Surrounding Rock, Foundation and Subgrade. *Sustainability* **2022**, *14*, 16947. [CrossRef]
47. Gao, Q.D.; Zhang, C.; Fan, Y.; Zhou, H.X.; Lu, W.B.; Leng, Z.D. Comparative analysis of blasting disturbance under different hole arrangement methods in pre-splitting excavation of gentle slope of dam-foundation. *J. Geotech. Eng.* **2023**, *56*, 7237–7254.
48. Feng, R.; Zhang, Y.; Rezagholilou, A.; Roshan, H.; Sarmadivaleh, M. Brittleness index: From conventional to hydraulic fracturing energy model. *Rock Mech. Rock. Eng.* **2020**, *53*, 739–753. [CrossRef]
49. He, W.; Chen, Z.; Shi, H.; Liu, C.; Li, S. Prediction of acoustic wave velocities by incorporating effects of water saturation and effective pressure. *Eng. Geol.* **2021**, *280*, 105890. [CrossRef]
50. Peng, N.; Ma, T.; Zhu, G.; Su, Q. Anti-drilling ability of Ziliujing conglomerate formation in Western Sichuan Basin of China. Petroleum. *Petroleum* **2022**, *9*, 41–52. [CrossRef]
51. Xia, K.; Chen, C.; Wang, T.; Zheng, Y.; Wang, Y. Estimating the geological strength index and disturbance factor in the Hoek–Brown criterion using the acoustic wave velocity in the rock mass. *Eng. Geol.* **2022**, *306*, 106745. [CrossRef]
52. Hoek, E.; Brown, E.T. The Hoek–Brown failure criterion and GSI—2018 edition. *Journal Rock Mech. Geotech. Eng.* **2018**, *19*, 445–463. [CrossRef]
53. Rinehart, J.S.; Fortin, J.P.; Burgin, L. Propagation velocity of longitudinal waves in rocks. Effect of state of stress, stress level of the wave, water content, porosity, Temperature, Stratification and Texture. In Proceedings of the 4th U.S. Symposium on Rock Mechanics (USRMS), Arma, PE, USA, 30 March–1 April 1961.
54. You, M.Q.; Su, C.D.; Li, X.S. Study on the relationship between mechanical properties of damaged rock samples and longitudinal wave velocity. *J. Rock Mech. Eng.* **2008**, *27*, 458–467.
55. Rezaei, M.; Davoodi, P.K.; Najmoddini, I. Studying the correlation of rock properties with P-wave velocity index in dry and saturated conditions-ScienceDirect. *J. Appl. Geophys.* **2019**, *169*, 49–57. [CrossRef]
56. Barton, N.R. *Rock Quality, Seismic Velocity, Attenuation and Anisotropy. Rock Quality Seismic Velocity Attenuation & Anisotropy*; CRC Press: Boca Raton, FL, USA, 2007.
57. Brady, B.H.G.; Brown, E.T. *Rock Mechanics for Underground Mining*; Springer: Berlin/Heidelberg, Germany, 2006.
58. Warren, S.N.; Kallu, R.R.; Barnard, C.K. Correlation of the Rock Mass Rating (RMR) System with the Unified Soil Classification System (USCS): Introduction of the Weak Rock Mass Rating System (W-RMR). *Rock Mech. Rock Eng.* **2016**, *49*, 4507–4518. [CrossRef]

59. Wang, D.G.; Hu, T.J.; Ye, Y.C. Study on wave velocity difference of different frequencies in elastic wave testing of rock mass. In Proceedings of the National Academic Conference on Vibration Theory and Application, Hangzhou, China, 17–19 October 2007.
60. Chen, Z.L.; Zhou, J.W.; Cai, Y.P.; Sun, P.; Deng, C.J. Discussion on the value of disturbance factor when Hoek-Brown strength criterion is applied to engineering slopes. *J. Yangtze River Sci. Res. Inst.* **2020**, *37*, 72.
61. Yan, C.B.; Li, G.Q.; Chen, D.L.; Liu, Z.H.; Liu, J.L. Modified Hoek-Brown criterion formula based on cumulative damage effect of rock blasting. *Geotech. Mech.* **2011**, *32*, 2951–2956.
62. Yang, J.H.; Dai, J.H.; Yao, C.; Jiang, S.H.; Jiang, Q.H. Study on weakening law of mechanical parameters of rock mass in blasting excavation damage area of high rock slope. *J. Geotech. Eng.* **2020**, *42*, 968–975.
63. Liu, N.; Yuan, W.; Gao, L.; Bai, X.S.; Di, X.; Li, J.P.; Xu, J. Digital identification of joint information of rock slope and reconstruction of three-dimensional model-A case study of Nanzhang town slope in Shijiazhuang. *Sci. Technol. Eng.* **2023**, *23*, 941–952.
64. Ajalloeian, R.; Mohammadi, M. Estimation of limestone rock mass deformation modulus using empirical equations. *Bull. Eng. Geol. Environ.* **2014**, *73*, 541–550. [CrossRef]
65. Yin, X.L.; Su, H.Y.; Lei, G.R.; Liu, L.F.; Xiong, K.; Feng, Z.H. Estimation of mechanical parameters of ore and rock based on RMR and Hoek-Brown criterion. *Chem. Miner. Process.* **2020**, *49*, 15–18.
66. Zuo, J.; Shen, J. *The Hoek-Brown Failure Criterion—From Theory to Application*; Springer: Singapore, 2020.
67. Bi, H.; Zhang, Y.; Wang, X.; Chen, Z.; Yu, Z.; Yuan, J.; Zuo, G. Simulation study of effective pumping speed of divertor pumping system for CFETR with COMSOL Multiphysics. *Fusion Eng. Des.* **2023**, *194*, 113916. [CrossRef]
68. Selvaraj, V.K.; Subramanian, J.A. comparative study of smart polyurethane foam using RSM and COMSOL multiphysics for acoustical applications: From materials to component. *J. Porous Mater.* **2022**, *30*, 547–563. [CrossRef]
69. Jafari, A.; Vahab, M.; Broumand, P.; Khalili, N. An eXtended Finite Element Method Implementation in COMSOL Multiphysics: Thermo-Hydro-Mechanical Modeling of Fluid Flow in Discontinuous Porous Media. *Comput. Geotech.* **2023**, *159*, 105458. [CrossRef]
70. Zhang, L.; Zhang, L.L.; Chen, Y.; Wang, J.H. Stability analysis of rainfall infiltration slope considering the influence of subsurface erosion. *J. Geotech. Eng.* **2014**, *36*, 1680–1687.
71. Zhong, C.Y.; Cui, P.; Zhu, S.R.; Qin, Y.W.; Wu, L.Z. Analysis of the influence of plant root water absorption on the stability of unsaturated soil slope. *J. Soil Water Conserv.* **2022**, *36*, 99–105.
72. Zhang, X.R.; Ma, Y.X.; Zhang, W.Y. Stability analysis of root-soil composite soil slope in seasonal frozen soil area. *Sci. Technol. Eng.* **2023**, *23*, 1248–1253.
73. He, Y.; Li, B.; Du, X. Soil Slope Instability Mechanism and Treatment Measures under Rainfall—A Case Study of a Slope in Yunda Road. *Sustainability* **2023**, *15*, 1287. [CrossRef]
74. Pan, X.E. Study on the selection of elastic modulus and Poisson's ratio in slope stability calculation by strength reduction method. *J. Water Conserv. Constr. Eng.* **2014**, *12*, 55–59.

Disclaimer/Publisher's Note: The statements, opinions and data contained in all publications are solely those of the individual author(s) and contributor(s) and not of MDPI and/or the editor(s). MDPI and/or the editor(s) disclaim responsibility for any injury to people or property resulting from any ideas, methods, instructions or products referred to in the content.